THE JOURNAL OF PHYSICAL CHEMISTRY A

Article

pubs.acs.org/JPCA

S/G-1: An ab Initio Force-Field Blending Frozen Hermite Gaussian Densities and Distributed Multipoles. Proof of Concept and First Applications to Metal Cations

Robin Chaudret,[†,‡] Nohad Gresh,[§] Christophe Narth,[†,‡] Louis Lagardère,[†,‡,∥] Thomas A. Darden,[⊥] G. Andrés Cisneros,*[,#] and Jean-Philip Piquemal*[,†,‡]

[†]Sorbonne Universités, UPMC, Univ Paris 06, UMR 7616, Laboratoire de Chimie Théorique, case courrier 137, 4 place Jussieu, F-75005 Paris, France

[‡]CNRS, UMR 7616, Laboratoire de Chimie Théorique, case courrier 137, 4 place Jussieu, F-75005 Paris, France

[§]Laboratoire de Chimie et Biochimie Pharmacologiques et Toxicologiques, UMR 8601 CNRS, Unité de Formation et de Recherche Biomédicale, Université Paris Descartes, 45 rue des Saint-Pères, 75006 Paris, France

[∥]Sorbonne Universités, UPMC Univ. Paris 06, Institut du Calcul et de la Simulation, F-75005 Paris, France

[⊥]OpenEye Scientific Software, 9 Bisbee Court, Suite D, Santa Fe, New Mexico 87508, United States

[#]Wayne State University, Department of Chemistry, 5101 Cass Ave., Detroit, Michigan 48202, United States

S *Supporting Information*

ABSTRACT: We demonstrate as a proof of principle the capabilities of a novel hybrid MM′/MM polarizable force field to integrate short-range quantum effects in molecular mechanics (MM) through the use of Gaussian electrostatics. This lead to a further gain in accuracy in the representation of the first coordination shell of metal ions. It uses advanced electrostatics and couples two point dipole polarizable force fields, namely, the Gaussian electrostatic model (GEM), a model based on density fitting, which uses fitted electronic densities to evaluate nonbonded interactions, and SIBFA (sum of interactions between fragments ab initio computed), which resorts to distributed multipoles. To understand the benefits of the use of Gaussian electrostatics, we evaluate first the accuracy of GEM, which is a pure density-based Gaussian electrostatics model on a test Ca(II)−H_2O complex. GEM is shown to further improve the agreement of MM polarization with ab initio reference results. Indeed, GEM introduces nonclassical effects by modeling the short-range quantum behavior of electric fields and therefore enables a straightforward (and selective) inclusion of the sole overlap-dependent exchange-polarization repulsive contribution by means of a Gaussian damping function acting on the GEM fields. The S/G-1 scheme is then introduced. Upon limiting the use of Gaussian electrostatics to metal centers only, it is shown to be able to capture the dominant quantum effects at play on the metal coordination sphere. S/G-1 is able to accurately reproduce ab initio total interaction energies within closed-shell metal complexes regarding each individual contribution including the separate contributions of induction, polarization, and charge-transfer. Applications of the method are provided for various systems including the HIV-1 NCp7-Zn(II) metalloprotein. S/G-1 is then extended to heavy metal complexes. Tested on Hg(II) water complexes, S/G-1 is shown to accurately model polarization up to quadrupolar response level. This opens up the possibility of embodying explicit scalar relativistic effects in molecular mechanics thanks to the direct transferability of ab initio pseudopotentials. Therefore, incorporating GEM-like electron density for a metal cation enable the introduction of nonambiguous short-range quantum effects within any point-dipole based polarizable force field without the need of an extensive parametrization.

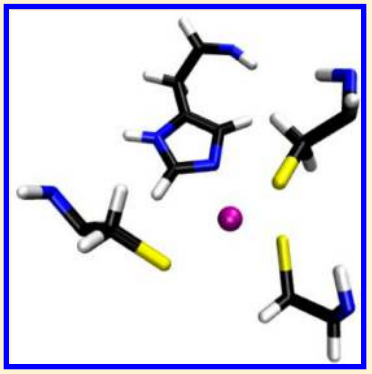

I. INTRODUCTION

Classical molecular mechanics (MM) models such as CHARMM,[1] AMBER,[2] or GROMOS[3] have been immensely valuable for the study of large biomolecular systems. While many successes have been obtained using these methods through long molecular dynamics (MD) simulations, there exist limits to their applicability, especially when dealing with metal cations. Indeed, it is quite difficult to discriminate two divalent cations by simply using different van der Waals parameters in the 6−12 Lennard-Jones interaction potential. In this context, new generation anisotropic polarizable molecular mechanics (APMM) methods have been introduced (see ref 4 and references therein). Among these, SIBFA (sum of interactions between fragment ab initio computed)[4] has been shown to be

Special Issue: Kenneth D. Jordan Festschrift

Received: May 29, 2014
Revised: May 29, 2014
Published: May 30, 2014

   dx.doi.org/10.1021/jp5051657 | J. Phys. Chem. A 2014, 118, 7598−7612

well suited for the treatment of Mg(II), Ca(II), Cu(I), Cu(II), and Zn(II) cations and their complexes in the recognition sites of metalloproteins[5,6] as well as for the treatment of heavy metals, up to lanthanides and actinides.[7] This method was designed following a "bottom-up" approach,[4] being grounded on gas-phase quantum chemistry. Indeed, in SIBFA, the first-order contributions (electrostatics and exchange-repulsion) and second-order polarization, charge-transfer, and dispersion energies are formulated to match their ab initio counterpart extracted from reference gas-phase intermolecular energy decomposition (EDA) computations since the method itself relies on the use of gas phase ab initio distributed multipoles and polarizabilities. Further refinements toward ab initio molecular mechanics using Gaussian electrostatics were recently introduced.[4,8−11] Thus, following the SIBFA philosophy, some of us proposed an ab initio force field using model electronic densities obtained from density fitting algorithms to replace the multipoles (or point charges). The Gaussian electrostatic model (GEM)[4,8−11] using Hermite Gaussian functions was shown to be particularly accurate in reproducing ab initio results in a framework enabling molecular dynamics.[10] It thus enabled highly accurate computations of intermolecular energies as well as improved boundaries for hybrid quantum mechanics/molecular mechanics (QM/MM) computations.[11] In this contribution, we propose a novel hybrid method, denoted S/G-1, which mixes SIBFA and GEM in order to increase the accuracy of the representation of the coordination sphere of metal ions.

Indeed, incorporating GEM-like electron density at the place of a metal cation should enable us to introduce nonambiguous short-range quantum effects without the need for an extensive parametrization. Upon introducing this methodology, we start by discussing the ability of a pure density-based MM scheme to accurately treat the polarization energy of a small metal complex. We then discuss the capability of the hybrid S/G-1 scheme, GEM being used only on the metal cation, to treat a large set of different benchmark computations going from transition to heavy metal cation complexes and from small systems to models of metalloproteins.

II. METHODS

A. Sum of Interaction Between Fragment ab Initio Computed (SIBFA) Procedure. SIBFA is a polarizable molecular mechanics procedure computed as a sum of five contributions, each of which is formulated and calibrated to reproduce its counterpart from an ab initio energy-decomposition analysis:

$$\Delta E_{\text{interaction}} = E_{\text{MTP}*} + E_{\text{exch/rep}} + E_{\text{pol}} + E_{\text{ct}} + E_{\text{disp}} \quad (1)$$

$E_{\text{MTP}*}$ is the Coulomb (i.e., electrostatic) energy. It is calculated from multipoles (up to quadrupoles) distributed on atoms and bond-midpoints. They are extracted from the molecular orbitals of the fragment thanks to a procedure due to Vigné-Maeder and Claverie.[12] $E_{\text{MTP}*}$ is corrected at short-range for electrostatic penetration errors using a damping function.[13]

$E_{\text{exch/rep}}$ is the short distance repulsion energy calculated as a sum of bond−bond, bond−lone pair, and lone pair−lone pair repulsions. The present form of the energy is grounded on an early theoretical work by Murrell et al.[14,15] and uses a formulation in $S^2/R + S^2/R^2$,[16] S being a function of the intermolecular overlap between the molecular orbitals localized on the bonds and the lone-pairs, and R the distance between the bond- or lone pair centroids. A 3-body correction is available and automatically included when dealing with metal centers.[17]

The sum of these two contributions forms the first order energy (denoted as E_1) contribution to the interaction energy.

E_{disp} represents the dispersion contribution to the interaction energy. It is coupled to an exchange-dispersion term and is computed as an expansion of Z^n terms: C_6/Z^6, C_8/Z^8 and C_{10}/Z^{10}, Z being expressed as

$$Z = \frac{r_{ij}}{\sqrt{W_A W_B}} \quad (2)$$

where r_{ij} is the distance between atoms i and j; and W_A and W_B are the effective radii of the involved atoms. The C_6, C_8, and C_{10} coefficients are empirical parameters adjusted on several H_2O dimers calculated at the SAPT level. Each one of the Z^n terms are damped at short-range.

The last two contributions are the focus of the new development illustrated in this article.

E_{pol} is the polarization energy.[18] In the context of SIBFA, the permanent electric fields are generated by multipoles and interact with distributed anisotropic dipolar polarizabilities derived by a procedure due to Garmer and Stevens.[19] These polarizabilities, denoted $\alpha_P(i,j)$, are 3×3 tensors located on the centroids of the Boys localized orbitals of each molecular fragment. This procedure offers the advantage that the induced dipoles within a molecule do not interact directly. The polarizabilities are computed with a modified version of HONDO 95.3[20] and have been shown to be a key ingredient for an accurate modeling of water within water chains.[21] We have then, for an induced and a permanent field (respectively, ΔE_{ind} and E_P)

$$\Delta\mu_P(i) = \sum_{j}^{xyz} (\alpha_P(i,j)(E_P(j) + \Delta E_{\text{induced}}(j)) \quad (3)$$

where $\Delta\mu_P(i)$ correspond to the induced dipoles leading to the polarization energy

$$E_{\text{pol}}(P) = -0.5 \sum_{i}^{xyz} \Delta\mu_P(i)(E_P(i)) \quad (4)$$

The iterative process for the electric field and effective radii leads to a more realistic model where the interactions between polarized points influence the values of different physical parameters including the polarization energy itself.

The parametrization of such contribution is detailed in the technical appendix.

E_{ct} is the charge-transfer energy[22] between each lone pair of fragment A acting as an electron donor and each electron acceptor orbital of a fragment B. The following expression was derived from the ab initio formulation due to Murrell et al.:[23]

$$E_{\text{ct}} = -2C \sum_{\alpha} \sum_{\beta*} N_{\text{occ}}(\alpha) \frac{(I_{\alpha\beta*})^2}{\Delta E_{\alpha\beta*}} \quad (5)$$

where α denotes the electron donor orbital (lone pair) and $\beta*$ denotes the electron acceptor orbital (virtual orbital). $N_{\text{occ}}(\alpha)$ is the occupation number of the orbital α, and C is a constant. $I_{\alpha\beta*}$ is a function of the overlap between the molecular orbital describing the donor lone pair and the antibonding virtual orbital of the electron acceptor bond, and of the electrostatic potential exerted on site A by all the other interacting

dx.doi.org/10.1021/jp5051657 | J. Phys. Chem. A 2014, 118, 7598−7612

molecules. $\Delta E_{\alpha\beta^*}$ is a function of the difference between the ionization potential of A and the electron affinity of B.

An extensive description of the charge-transfer equations is given in the technical appendix.

Overall, as one can see, SIBFA embodies more centers than atoms and can explicitly treat interactions due to local molecular orbitals interactions thanks to nonatomic centers.

B. Gaussian Electrostatic Model (GEM) Approach. The Gaussian electrostatic model (GEM) is based on the reproduction of the different components of the interaction energy just as SIBFA. The major differences are that the calculation of the Coulomb term is done with integrals, the exchange is calculated with the overlap model of Wheatley and Price,[24] and the electrostatic potentials and fields are done with frozen densities fitted to linear combinations of Gaussians or Hermite Gaussians using density-fitting methods.[25,26] In essence, the method relies on the use of an auxiliary Gaussian basis set to fit the molecular electron density obtained from an ab initio relaxed one-electron density matrix

$$\tilde{\rho} = \sum_{k=1}^{N} x_k k(r) \approx \rho = \sum_{\mu\nu} P_{\mu\nu}\phi_\mu(r)\phi_\nu^*(r) \tag{6}$$

To do so, a variational density fitting treatment[25,26] that minimizes the Coulomb self-interaction energy of the error is performed:

$$E_2 = \frac{1}{2}\iint \frac{[\rho(r_1) - \tilde{\rho}(r_1)][\rho(r_2) - \tilde{\rho}(r_2)]}{|r_1 - r_2|} dr_1 dr_2$$
$$= \langle \rho - \tilde{\rho} \,||\, \rho - \tilde{\rho} \rangle \tag{7}$$

Inserting the right-hand side of eq 6 into eq 7 we obtain

$$E_2 = \frac{1}{2}\sum_{\mu,\nu}\sum_{\sigma,\tau} P_{\mu\nu}P_{\sigma\tau}\langle\mu\nu||\sigma\tau\rangle - \sum_l x_l \sum_{\mu,\nu} P_{\mu\nu}\langle\mu\nu||l\rangle + \frac{1}{2}\sum_k\sum_l x_k x_l \langle k\,||\,l\rangle \tag{8}$$

E_2 from eq 8 can be minimized with respect to the expansion coefficients x_l, and a linear system of equations can be obtained

$$\frac{\partial E_2}{\partial x^l} = -\sum_{\mu\nu} P_{\mu\nu}\langle\mu\nu\,||\,l\rangle + \sum_k x_k \langle k||l\rangle \tag{9}$$

Equation 9 is used to determine the coefficients

$$x = A^{-1}b \tag{10}$$

where

$$b_l = \sum_{\mu\nu} P_{\mu\nu}\langle\mu\nu\,||\,l\rangle \text{ and } A_{kl} = \langle k\,||\,l\rangle \tag{11}$$

These coefficients can be used directly as a new object to compute directly Coulomb and exchange/repulsion energies between interacting frozen densities but can also be used to compute electrostatic fields and potentials. To preserve accuracy due to noise in the fitting procedure, many strategies have been tested and are described elsewhere.[9]

Moreover, the choice of auxiliary basis sets is not restricted to Cartesian Gaussians, and Hermite Gaussian functions are preferred as they offer the possibility to use directly efficient McMurchie−Davidson (McD)-like recursions.[27] In addition, the fitted Hermite Gaussians are closely related to multipoles since they have a simple relation to elements of the Cartesian multipole tensor, which allows the direct calculation of distributed multipoles from the Hermite Gaussians.[9] This offers a smooth connection defining a continuous electrostatic model that can be used directly for second generation APMM force fields such as SIBFA and AMOEBA.[28]

In the present implementation, we will still continue to use the multipoles built within the SIBFA framework obtained with the Vigné-Maeder−Claverie approach but technically the GEM multipoles could be used to perform all electrostatic computations.

C. Quantum Chemical Calculations. Energy-decomposition analyses were performed using the constrained space orbital variations (CSOV)[29] and reduced variational space (RVS) methods,[30] using the HONDO 95.3[20] and GAMESS[31,32] packages, respectively. The ab initio reference level (Hartree−Fock/CEP 4-31G(2d))[33] was chosen in order to be consistent with previous SIBFA studies. The initial CEP-431G is enriched by two 3d polarization functions. This enables the CEP 4-31(2d) basis to yield interaction energies, which at the HF level are very close to those from larger basis sets.[34]

Additional CSOV computations were performed at the B3LYP/aug-cc-pVTZ (water)/6-31G**(metal) level[35,36] in the cases of the pure GEM computations. The same level of theory was used for the derivation of the distributed multipoles, densities, and polarizabilities. All fitting coefficients were obtained with an in-house Fortran-90 program.

III. IMPROVED TREATMENT OF METAL CATIONS USING GAUSSIAN ELECTROSTATICS

A. Importance of Short-Range Effects in the Treatment of Induction Energies: Full Gaussian Electrostatic Treatment. *1. Unravelling Physical Effects.* Energy decomposition analysis (EDA) literature concur to the need for induction to embody both polarization and charge-transfer energies when converging to the basis set limit (see ref 37 for a detailed discussion about scheme equivalence). However, two limitations should be associated with this assumption. First, charge-transfer is more complex than a simple basis set artifact. Indeed, with transition and heavy metal complexes it is associated with the physical donation and back-donation[38] between metal and ligand occupied and virtual orbitals. Second, even for nonmetallic systems, quantum mechanical computations are virtually never performed at the basis set limit for medium and large-size molecules leading to a significant charge-transfer term, which cannot be accurately modeled by the sole polarization component. For large systems, molecular mechanics models must separately reproduce the two distinct parts of the induction energy (or at least incorporate charge-transfer into the van der Waals contribution in order to avoid spurious polarization overfitting.[39] Unfortunately, in addition to this already difficult situation, ab initio reference polarization and charge-transfer energies embody "repulsive", exchange-polarization, and exchange-charge-transfer ($E_{\text{exch-pol}}$ and $E_{\text{exch-ct}}$) counterparts. Such terms account for the second-order Pauli repulsion, which arise from the need of an antisymmetrized total wave function (i.e., to overcome an overestimation of the induction energy [see ref 37 for discussion]).

We then have

$$E_{\text{ind}} = E_{\text{pol}} + E_{\text{exch-pol}} + E_{\text{ct}} + E_{\text{exch-ct}} \tag{12}$$

The problem then becomes very complex if one attempts to compute these terms using a classical approach such as a force-

dx.doi.org/10.1021/jp5051657 | J. Phys. Chem. A 2014, 118, 7598−7612

field; the question of short-range electrostatics becomes a key issue. Similar to the Coulomb energy, the polarization energy cannot be fully formulated using a multipolar approximation since penetration effects occur at short-range due to molecular orbital overlap. Thus, the total induction energy can be rewritten as follows:

$$E_{ind} = E_{pol(classical/multipolar)} + E_{pol(short\text{-}range\ penetration)} + E_{exch\text{-}pol} + E_{ct} + E_{exch\text{-}ct} \quad (13)$$

We then have three different physical effects present in the ab initio polarization contribution: (1) the classical (multipolar) polarization; (2) the exchange-polarization (part of the second-order Pauli exchange term); and (3) the short-range penetration contribution.

$$E_{pol} = E_{pol(classical/multipolar)} + E_{pol(short\text{-}range\ penetration)} + E_{exch\text{-}pol} \quad (14)$$

Therefore, in order to accurately model induction, molecular mechanics treatments have to include all these components within their formalism. We will see in the next section that the use of Gaussian Hermite densities can provide some insights on the capabilities of molecular mechanics to include all these effects.

2. Ca(II)–H_2O as a Test System: Full Gaussian Electrostatics Treatment Using GEM. In order to try to include the different previously discussed physical effects within a MM scheme, we show here some results focusing on the polarization contribution in the case of the Ca(II)–H_2O complex.

Figure 1 displays four curves, namely, the reference ab initio CSOV polarization contribution, the "undamped" full GEM polarization energy, the "full GEM + damping" approach, and results obtained upon computing the polarization energy obtained with the exact ab initio undamped field values extracted from a quantum mechanical computation using the Gaussian 09 software.[40] The damping procedure is identical to the one used by SIBFA and is detailed in the technical appendix.

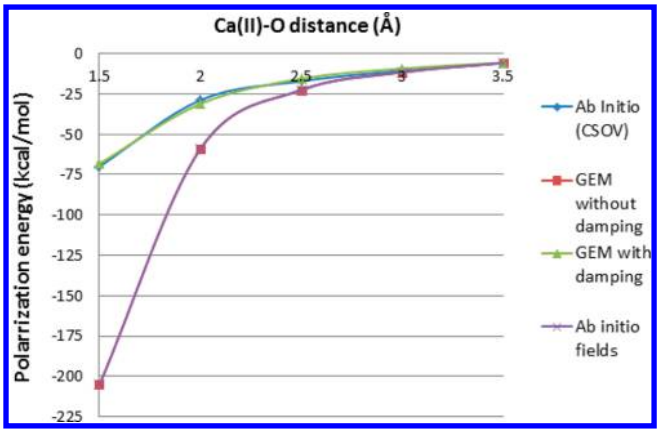

Figure 1. Ca(II)–H_2O complex. Ab initio polarization energies (kcal/mol) computed using the CSOV procedure (blue) and polarization energy computed using distributed polarizabilities + ab initio fields (gray), distributed polarizabilities + GEM with (green), and without fields damping (red) .

Here, it is important to point out that the GEM fields alone, in spite of their quasi-perfect match with their ab initio counterparts, do not enable a good reproduction of ab initio results at short-range: a damping of the fields is required to gain accuracy at very short distances. Such conclusions are confirmed as our results obtained from "undamped" exact ab initio fields (i.e., computed using the original molecular orbitals) are basically identical to the undamped GEM results (see Figure 1). This clearly shows that inclusion of short-range quantum effects, inherently present within QM and GEM fields, is not sufficient to reproduce the true polarization energy. This is because the final ab initio CSOV polarization energy embodies both penetration *and* exchange-polarization effects. If the first quantity is present in GEM (as in QM), the exchange-polarization arises from the required orthogonalization[37] of molecular orbitals of both Ca(II) and H_2O fragments within the constrained self-consistent field procedure. Therefore, as GEM is not including this repulsive effect, the computed polarization energy is overestimated. A straightforward solution to the problem is to apply the exact same field damping procedure that is used for the SIBFA polarization contribution. As we can see from Figure 1, the "GEM + damping" approach accurately reproduces the CSOV reference by selectively including the different effects.

B. Hybrid S/G-1 Approach for Polarization and Charge-Transfer Energies. *1. Multiscale S/G-1 Approach.* In this initial implementation the direct coupling between GEM and SIBFA has been only performed at the induction level (polarization and charge-transfer energies) in the spirit of QM/MM techniques.

Indeed, the GEM equations for exchange-repulsion involve overlap integrals between densities of *both* interacting fragments. Thus, a mixed S/G-1 scheme is not possible for E_{rep} as the overlap of a GEM density with SIBFA's multipoles would be null. Therefore, in the present S/G-1 implementation, the electrostatic, exchange-repulsion, and dispersion energies are computed at the sole SIBFA level but include the SIBFA short-range corrections. In a forthcoming work, the full multiscale implementation including full Gaussian electrostatics first order energy will be reported. Therefore, in this contribution, GEM is presently only used to compute the second-order E_{pol} and E_{ct} contributions between the cation and its bound ligands. Finally, the dispersion equations are the same for both methods, as they do not depend on electric fields or potentials. As a proof of concept, we will limit ourselves to a Hartree–Fock level parametrization (no dispersion) of the method in this contribution.

Summarizing, within S/G-1, the evaluation the polarization and charge-transfer energies use the same formalism. The differences between the two levels of computations relate to the level of calculation of electric fields and potentials, namely, using electronic densities for GEM or using distributed multipoles for SIBFA. Indeed, differences between GEM and SIBFA fields and potentials can arise at short distances since the GEM potential is nearly identical to the ab initio one. Both procedures converge to the same solutions upon increasing the distances when the multipolar approximation starts to be valid as GEM densities act as a continuous electrostatic model. Therefore, in a similar spirit as in QM/MM approaches, specific fragments can be defined so as to be handled with either the GEM density or the SIBFA multipoles.

For the present study, the use of GEM densities is restricted to the metal cations, whereas the rest of the molecules is described using SIBFA.

dx.doi.org/10.1021/jp5051657 | J. Phys. Chem. A 2014, 118, 7598–7612

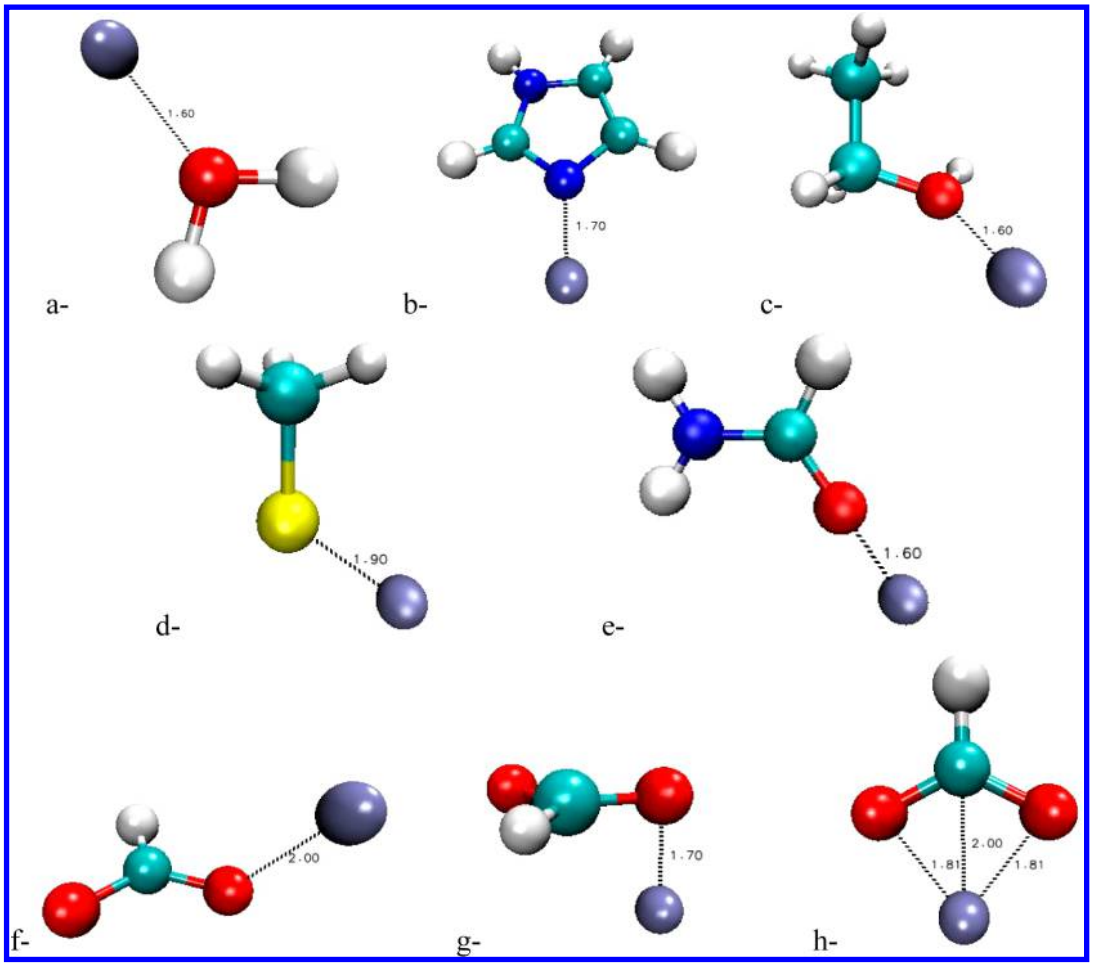

Figure 2. Representation of the monoligated zinc complexes used to calibrate SIBFA within the S/G-1 context: (a) $[Zn(H_2O)]^{2+}$, (b) $[Zn(imidazole)]^{2+}$, (c) $[Zn(ethanol)]^{2+}$, (d) $[Zn(CH_3S)]^{+}$, (e) $[Zn(formamide)]^{2+}$, (f) $[Zn(formate\ external)]^{+}$, (g) $[Zn(formate\ orthogonal)]^{+}$, and (h) $[Zn(formate\ bidendate)]^{+}$.

2. Calibration of the S/G-1 Approach for Zn(II) and Hg(II). a. Calibration of the Divalent Zn(II) Cation. S/G-1 was calibrated by using a series of representative monoligated zinc complexes (Figure 2). Following refs 18 and 41, the values of E_{pol} and E_{ct} were computed by varying the cation−ligand distances in 0.1 Å increments (see Tables in Supporting Information).

We tested the approach at very short distances that are usually far below those found at energy-relevant distances. However, such short distances can be found along a MD trajectory and could affect free energy computations or MD computed properties. Therefore, it is a favorable feature from this work that reasonable agreements are still obtained by the method at such distances.

Consistent with this work, both in- and out-of-plane Zn binding modes were considered upon formate binding. We have then considered both the bidentate mode, in which Zn(II) is along the internal bisector of the OCO angle, and the monodentate mode, in which one Zn−O distance is held at 2.0 Å, while the C−O−Zn is varied in steps of 15° steps from 90° to 180° (Figure 2g). Such representative complexes enable to test the calibration upon dealing with neutral as well as anionic ligands, with different lone-pair types (i.e., σ, sp^3, sp^2, and π). It also allows testing the sensitivity of each energy contribution to orientation in the case of cation−formate binding. The new parameters obtained are reported in the Supporting Information.

b. Calibration of the Divalent Hg(II) Cation. In order to further evaluate this novel methodology, we undertook a calibration of a heavy metal cation, namely, the divalent mercury cation Hg(II), where both relativistic and correlation effects come into play. Such a metal was recently studied within the context of SIBFA as we showed that very various physical effects were important including some 3-body terms within metal−ligand exchange-repulsion.[17] Our purpose is here to illustrate the ability of the S/G-1 procedure to accurately model such a challenging cation, rather than deriving a definitive set of parameters for it. Following ref 20, the parameters were fitted on three oligo-ligated complexes of Hg(II) with water, which are represented in Figure 3. Both E_{MTP*} and E_{rep} at first-order and E_{ct} at second-order were calibrated on the monoligated Hg(II)—H_2O complex in order to match their RVS counterparts upon varying the Hg−O distances from 1.8 to 2.9 Å.

The calibration of the cation polarization energy was less straightforward, as it embodies two components. The first stems from the cation dipolar polarizability and depends on the electrostatic field it experiences. The second stems from the quadrupolar polarizability and depends on the field gradient.[42] The magnitude of the second component was found to be important in the case of some metal cations, such as Cu(I), and this component had then to be explicitly formulated in

dx.doi.org/10.1021/jp5051657 | J. Phys. Chem. A 2014, 118, 7598−7612

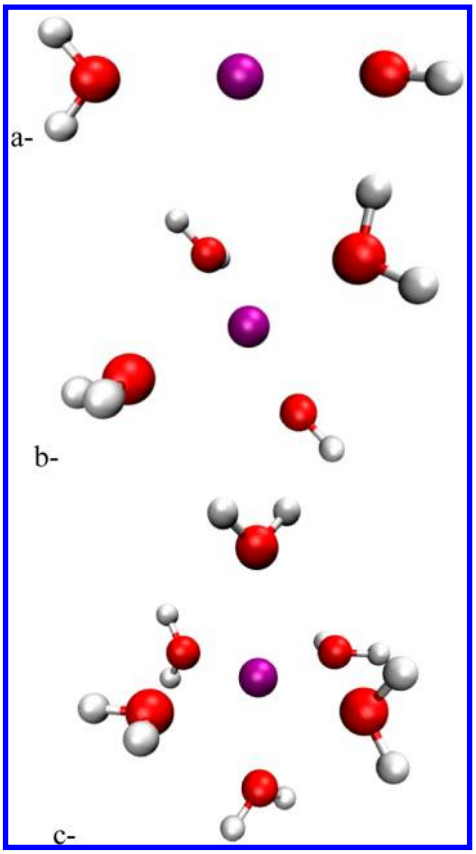

Figure 3. Representations of the water−Hg(II) polyligated complexes: (a) $[Hg(H_2O)_2]^{2+}$, (b) $[Hg(H_2O)_4]^{2+}$ pyramidal, and (c) $[Hg(H_2O)_6]^{2+}$ octahedral.

SIBFA.[43] This is also the case for Hg(II).[17] The reference quantum value of Hg(II) dipolar polarizability can be easily obtained; however, its quadrupolar polarizability could not be derived by QM calculations using a small core pseudopotential. Therefore, we resorted to the available Cu(I)[43] value as a starting point. The values of E_{pol}(Hg) were obtained from an RVS calculation done on the $[Hg(H_2O)_2]^{2+}$ complex, with Hg(II) equidistant from the two water molecules. In such a complex, the field undergone by Hg(II) is null, but the gradient is non-null. We thus scaled the Cu(I) quadrupolar polarizability in order to best match the evolutions of E_{pol}(Hg(II)) for Hg−O distances in the 2.1—2.6 Å range.

IV. RESULTS

A. Mono- and Polyligated Zn(II) Complexes: Toward Zn(II)−Metalloproteins Simulations. For all monoligated complexes, the radial evolutions of E_{pol} and E_{ct} are reported in Table S1 of the Supporting Information. Table 1 reports the values of both contributions at equilibrium distance. Figure 4 illustrates the radial evolutions of E_{pol} and E_{ct} for the Zn−water and Zn−formamide complexes, as computed by RVS, S/G-1, and SIBFA procedures.

Please note that E_{pol}* corresponds to the polarization energy prior to iterating on the induced dipoles and their effects on the polarizing fields. E_{pol} is the fully relaxed polarization. E_{pol}* can be compared to RVS, while E_{pol} can be compared to the fully relaxed variational-like polarization.

The values of E_{ct} are seen to not change significantly upon going from SIBFA to S/G-1 even at short distances (see Figure 4b,d for Zn−water and Zn−formamide complexes). They are virtually equal at equilibrium distances. Thus, for the Zn−ethanol complex at 1.9 Å, E_{ct}^{SIBFA} and $E_{ct}^{S/G-1}$ amount to −10.1 and −10.2 kcal/mol, respectively, whereas E_{ct}^{RVS} amounts to −11.9 kcal/mol. This shows that the electrostatic potentials and fields computed in SIBFA within a multipolar approximation, appearing in the expression of E_{ct}, already enable a close reproduction of the corresponding E_{ct}^{GEM} term, which uses densities instead.

However, the E_{pol} values at equilibrium and shorter distances appear strongly improved as depicted in Figure 4a,c. Thus, regarding the Zn−ethanol complex, E_{pol}^{RVS} amounts to −52.0 kcal/mol and E_{pol}^{SIBFA} amounts to −47.9 kcal/mol, whereas $E_{pol}^{S/G-1}$ amounts to −51.3 kcal/mol. Indeed, at short distance, the multipolar expansion performed for the calculation of electric fields and potentials in SIBFA starts to reach its limit, so that using a frozen density electric field correspondingly improves the treatment of E_{pol}. Moreover, within SIBFA, both short-range electric field quantum behavior and exchange-polarization have to be handled through damping, whereas GEM already embodies the first effect leading to an easier

Table 1. Values of the Polarization and Charge-Transfer Energies in kcal/mol for All Monoligated Complexes at Their Equilibrium Distances

		RVS				S/G-1			
complexes	distance (Å)	E_{pol}*	E_{pol}	E_{ct}	E_2	E_{pol}*	E_{pol}	E_{ct}	E_2
$[Zn(H_2O)]^{2+}$	1.90	−37.5	−39.2	−9.49	−48.7	−37.3	−38.8	−10.26	−49.0
$[Zn(imidazole)]^{2+}$	1.90	−71.4	−74.4	−21.4	−95.2	−70.3	−74.3	−20.6	−94.9
$[Zn(ethanol)]^{2+}$	1.90	−52.0	−54.2	−11.9	−66.1	−51.3	−52.3	−10.1	−62.3
$[Zn(CH_3S)]^{+}$	2.20	−79.6	−84.8	−47.8	−123.6	−78.2	−83.9	−50.0	−134.0
$[Zn(formate\ bidendate)]^{+}$	1.97	−70.8	−75.1	−22.0	−97.1	−72.1	−75.7	−24.6	−100.3
$[Zn(formamide)]^{2+}$	1.9	−57.6	−59.9	−9.4	−69.3	−58.1	−59.6	−8.5	−68.1
		RVS				SIBFA			
complexes	distance (Å)	E_{pol}*	E_{pol}	E_{ct}	E_2	E_{pol}*	E_{pol}	E_{ct}	E_2
$[Zn(H_2O)]^{2+}$	1.90	−37.5	−39.2	−9.49	−48.7	−34.9	−36.1	−10.49	−46.7
$[Zn(imidazole)]^{2+}$	1.90	−71.4	−74.4	−21.4	−95.2	−69.7	−73.5	−20.5	−94.1
$[Zn(ethanol)]^{2+}$	1.90	−52.0	−54.2	−11.9	−66.1	−47.9	−48.7	−10.2	−58.8
$[Zn(CH_3S)]^{+}$	2.20	−79.6	−84.8	−47.8	−123.6	−77.2	−82.1	−49.9	−132.0
$[Zn(formate\ bidendate)]^{+}$	1.97	−70.8	−75.1	−22.0	−97.1	−68.4	−70.7	−24.5	−95.5
$[Zn(formamide)]^{2+}$	1.9	−57.6	−59.9	−9.4	−69.3	−54.6	−56.7	−8.6	−65.3

dx.doi.org/10.1021/jp5051657 | J. Phys. Chem. A 2014, 118, 7598−7612

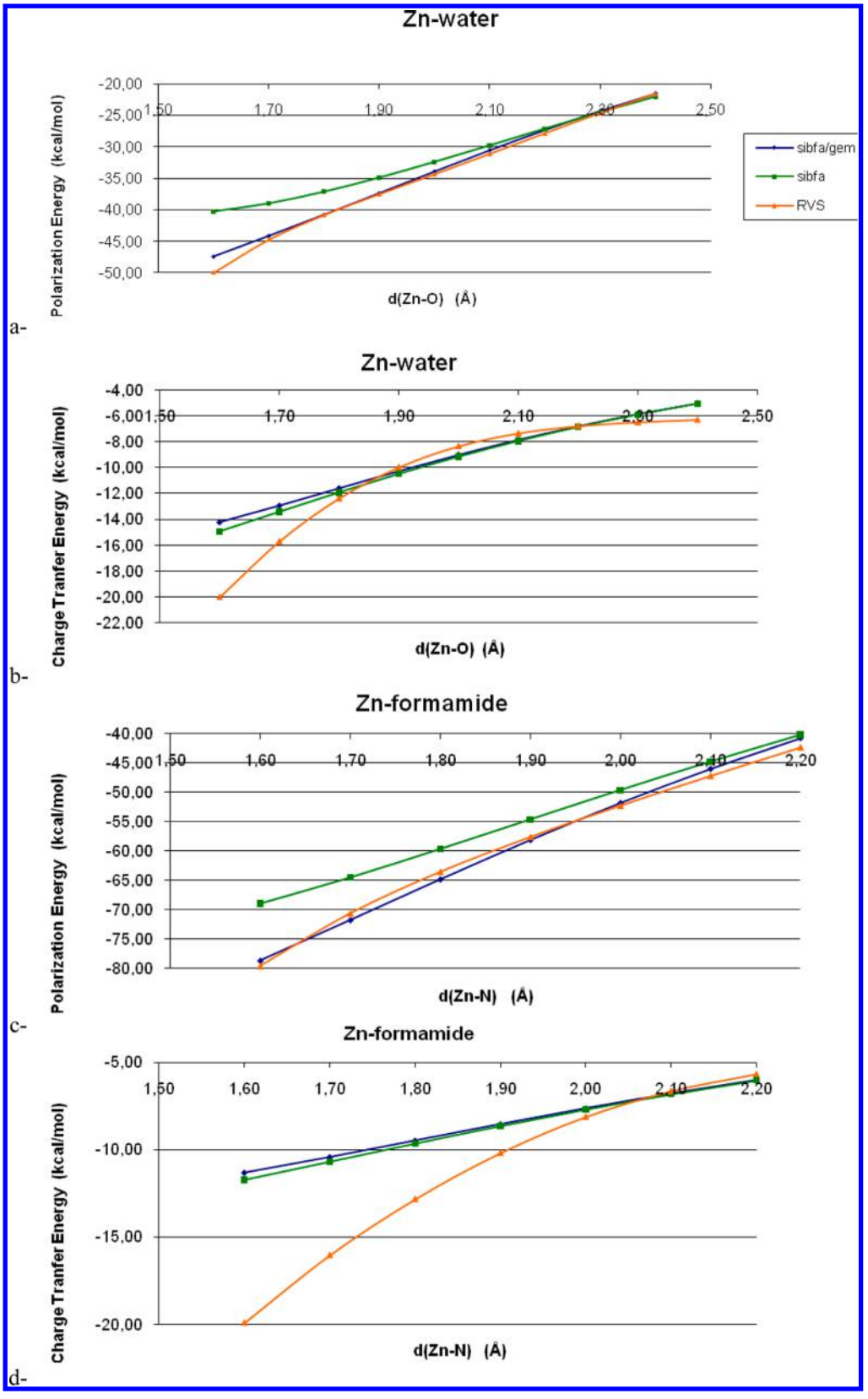

Figure 4. Zn−water. Distance evolutions of (a) E_{pol} as computed by RVS, SIBFA, and S/G-1 and (b) of E_{ct}. Zn−formamide. Corresponding distance evolutions of (c) E_{pol} and (d) E_{ct}. The RVS, SIBFA, and S/G-1 curves are represented with orange triangles, green squares, and blue diamonds, respectively.

correction of the sole exchange-polarization effects by damping. It is important to point out that in contrast to the full GEM implementation presented in the previous section the S/G-1 approach, which is limited to the use of Gaussian electrostatics for the metal cation, is able to recover the main physical effects.

dx.doi.org/10.1021/jp5051657 | J. Phys. Chem. A 2014, 118, 7598−7612

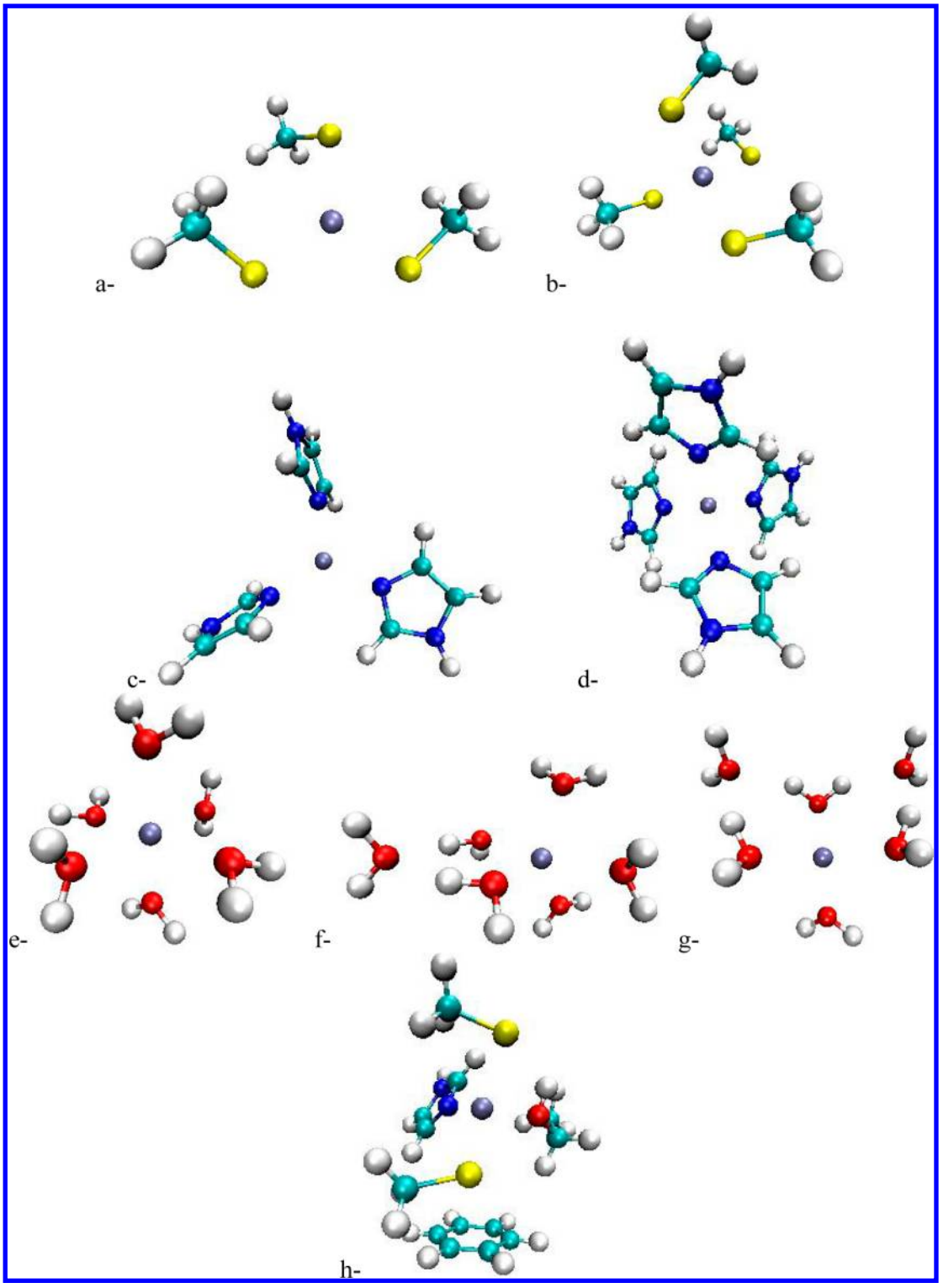

Figure 5. Representation of the polyligated zinc complexes in N, O, and S-ligands: (a) $[ZN(CH_3S)_3]^-$, (b) $[ZN(CH_3S)_4]^{2-}$, (c) $[Zn(imidazole)_3]^{2+}$, (d) $[Zn(imidazole)_4]^{2+}$, (e) $[Zn(H_2O)_6]^{2+}$, (f) $[Zn(H_2O)_{5/1}]^{2+}$, (g) $[Zn(H_2O)_{4/2}]^{2+}$, and (h) ADH. The ADH complex represents the active site of the alcohol dehydrogenase enzyme.

This attests to the importance of short-range quantum effects involving the metal cation.

We have next considered polyligated Zn complexes with N, O, and S ligands (Figure 5). This should enable the evaluation of the robustness of S/G-1 and, in particular, if it can account for the nonadditivity of both E_{pol} and E_{ct} upon passing from mono- to oligoligated complexes of Zn(II). The values of E_{pol} and E_{ct} are given in Table 2. S/G-1 matches the anticooperative behavior of E_{pol} and E_{ct}^{RVS}. Thus, for $[Zn(H_2O)_{4/2}]^{2+}$, $E_{ct}^{S/G-1}$ amounts to −26.8 kcal/mol, while E_{ct}^{RVS} amounts to −28.7 kcal/mol. Correspondingly, $E_{pol}^{S/G-1}$ amounts to −103.8 kcal/mol as compared to −101.7 kcal/mol concerning E_{pol}^{RVS}.

As a test of the applicability of S/G-1 to large systems, we applied this method to two Zn(II)-dependent systems recently

dx.doi.org/10.1021/jp5051657 | J. Phys. Chem. A 2014, 118, 7598−7612

Table 2. Values of the RVS and S/G-1 Polarization and Charge-Transfer Energies in Polyligated Zn(II) Complexes[a]

	RVS				S/G-1			
complexes	E_{pol*}	E_{pol}	E_{CT}	E_2	E_{pol*}	E_{pol}	E_{CT}	E_2
$[Zn(H_2O)_6]^{2+}$	−104.2	−85.4	−16.9	−102.2	−108.9	−84.3	−21.3	−105.7
$[Zn(H_2O)_{5/1}]^{2+}$	−112.5	−96.0	−20.9	−116.9	−115.3	−94.8	−24.1	−118.9
$[Zn(H_2O)_{4/2}]^{2+}$	−118.7	−105.1	−25.3	−130.4	−120.2	−103.8	−26.8	−130.5
$[Zn(CH_3S)_3]^{-}$	−95.6	−74.9	−47.8	−122.7	−99.4	−85.3	−44.9	−130.2
$[Zn(CH_3S)_4]^{2-}$	−68.0	−50.1	−37.8	−87.1	−65.0	−50.0	−45.3	−95.3
$[Zn(imidazole)_3]^{2+}$	−158.3	−133.0	−37.7	−170.8	−157.9	−136.1	−28.8	−164.9
$[Zn(imidazole)_4]^{2+}$	−170.8	−132.7	−37.2	−169.9	−172.2	−132.3	−29.2	−161.5
ADH	−113.2	−85.5	−43.4	−128.9	−125.6	−98.7	−40.8	−139.5

[a]Values for polarization, charge-transfer, and global second order (induction) energies in kcal/mol. E_{CT} and E_2 energies include a BSSE correction. Two different polarization energies are introduced here for ab initio calculations and S/G-1 calculations.

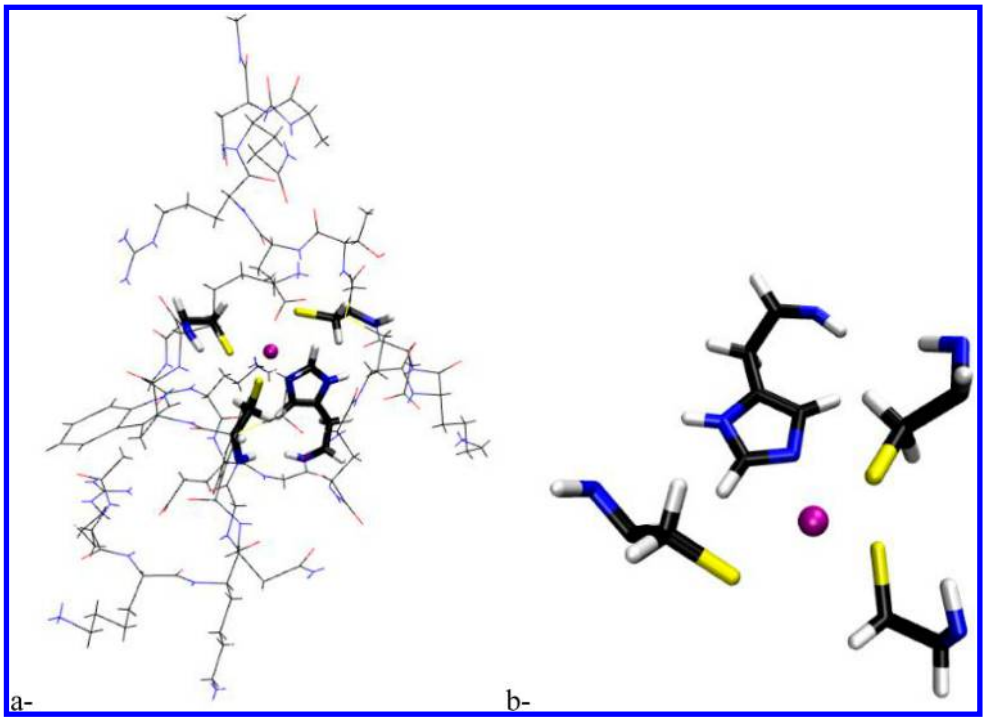

Figure 6. Representation of (a) the C-terminal end of the NCp7 Zn(II) finger and (b) its Zn(II) binding site.

studied with SIBFA. Here, the Zn(II)−alcohol dehydrogenase (ADH) active site[5] was modeled (see Figure 5h), using GEM to model Zn(II) while the ADH residues were treated with SIBFA. Such difficult heteropolyligated complex was modeled with success in S/G-1 with results on second order being less than 10% away from the ab initio reference. This first step toward the S/G-1 modeling of large biological systems was followed by the first study of a large oligopeptide, namely, the C-terminal Zn(II) finger of the HIV-1 nucleocapsid protein (NCP7), which encompasses 23 residues (see Figure 6).[6] NCP7 plays a crucial role in HIV-1 structural stability and for its stability for its integration into the host cell and is regarded as a potential target for the development of antiviral drugs. Interaction energies between NCP7 and its ligand at the SIBFA and S/G-1 levels are provided in Table S3 in the Supporting Information. These two last examples show that the S/G-1 method could have concrete applications in metalloprotein modeling as long as breaking and forming of bonds are not studied.

B. Hg(II) and Treatment of Relativistic Effect within the S/G-1 Approach. Another asset of the hybrid S/G-1 approach is its ability to reproduce the energetic properties of heavy metal cation complexes since it offers ways to deal with the effects of both relativity and electronic correlation. We present here the first S/G-1 implementation of the divalent Hg(II) mercury cation. Figure 7 displays, for the Hg(II)−H_2O complex, the distance evolutions of the individual ΔE contributions. Except at very short distances, the error between S/G-1 and SIBFA with respect to the ab initio calculations remains very small. As previously observed for the monoligated Zn(II) complexes, the S/G-1 and SIBFA values of E_{ct} are very close to one another. Again, the main differences arise from the values of E_{pol}. As observed for the Zn(II) complexes, S/G-1 remains closer to E_{pol}^{QC} than SIBFA at short-range. Figure 7e shows that $\Delta E^{S/G\text{-}1}$ has an improved agreement with respect to ΔE^{QC} than ΔE^{SIBFA}. Nevertheless, both curves remain close to the QC one.

Complexes with more than one water molecule, namely, $[Hg(H_2O)_2]^{2+}$, $[Hg(H_2O)_4]^{2+}$, and $[Hg(H_2O)_6]^{2+}$, were subsequently investigated. The results are reported in Tables 3 and 4. The close agreement found for the monoligated complex is retained with the polyligated ones. Therefore, the

dx.doi.org/10.1021/jp5051657 | J. Phys. Chem. A 2014, 118, 7598−7612

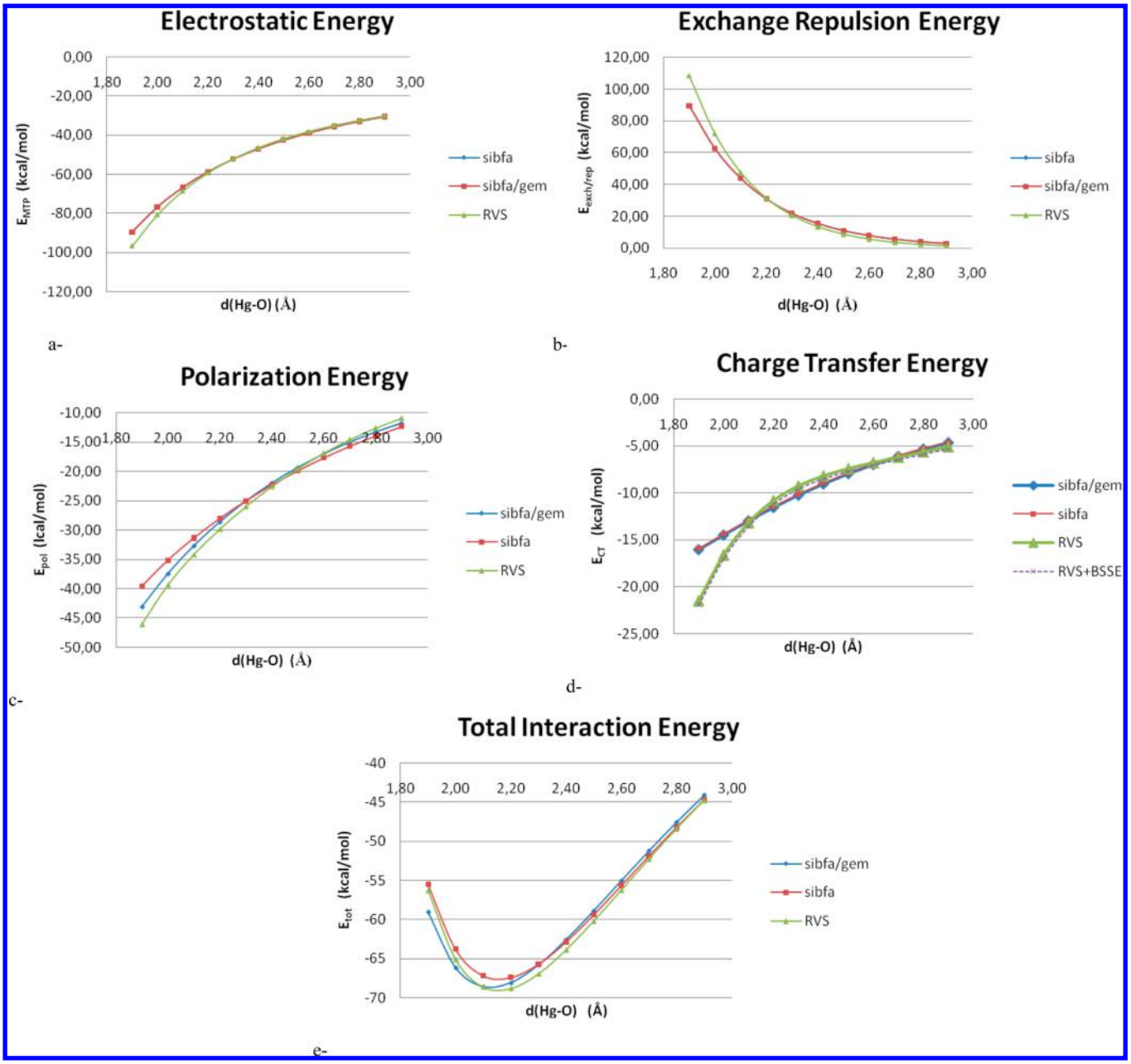

Figure 7. $[Hg(H_2O)]^{2+}$ complex. Variation as a function of the Hg−O distance of the SIBFA, S/G-1, and ab initio (RVS) values of the different contributions of the interaction energy (a, electrostatic energy; b, exchange-repulsion energy; c, polarization energy; d, charge-transfer energy; and e, global interaction energy) with the distance between the cation Hg^{2+} and the oxygen atom of the water molecule.

nonadditivity of both E_{pol} and E_{ct} can be reproduced with S/G-1 for Hg(II) and is consistent with previous results on Zn polyligated complexes.This is exemplified in the case of the hexahydrate $[Hg(H_2O)_6]^{2+}$. Upon multiplying by six the number of water ligands, E_{pol} and E_{ct}(QC) increase by factors of only 3.6 and 2.4, respectively. The corresponding increases of $E_{pol}^{S/G-1}$ and $E_{ct}^{S/G-1}$ are 3.8 and 3.0, respectively.

V. CONCLUSION AND PERSPECTIVES

The present article has reported the development of the ab initio S/G-1 force field. It blends together GEM, which embodies treatment of short-range quantum effects through the use of Gaussian electrostatics, and SIBFA, which resorts to distributed ab initio multipoles. We have considered several mono- and polyligated complexes of closed-shell metal cations. S/G-1 was shown to accurately reproduce polarization/charge-transfer (induction) from from ab initio EDA as well as total interaction energies within closed-shell metal complexes. We first showed that a pure Gaussian electrostatics model such as GEM can perform even better than a purely multipolar model because it selectively and explicitly embodies nonclassical effects in the expression of the polarizing fields. This allows a separate inclusion of exchange-polarization effects through damping. By contrast, in a multipolar method, both short-range electric field quantum behavior and exchange polarization have to be handled through damping. Furthermore, Gaussian electrostatics opens the possibility of including explicit scalar relativistic effects in molecular mechanics through a direct transferability of ab initio pseudopotentials. It was found, that the use of ab initio quality GEM potentials does not lead to a

dx.doi.org/10.1021/jp5051657 | J. Phys. Chem. A 2014, 118, 7598−7612

Table 3. $[Hg(H_2O)_2]^{2+}$ Complex[a]

distance (Å)	2.10		2.20	
$[Hg(H_2O)_2]^{2+}$	RVS	S/G-1	RVS	S/G-1
E_{MTP*}	−135.6	−132.1	−117.2	−113.8
$E_{exch/rep}$	95.8	87.2	63.3	59.0
E_1	**−39.8**	**−44.9**	**−53.9**	**−54.8**
E_{pol*}	−61.4	−50.8	−53.6	−46.3
E_{pol} ($E_{pol\ quad}$)	−68.6	−65.1 (−14.8)	−58.5	−56.4 (−10.6)
E_{CT}	−25.2	−20.8	−20.2	−18.7
E_2	**−93.8**	**−85.9**	**−78.8**	**−75.1**
ΔE	***−133.6***	***−130.8***	***−132.7***	***−130.0***
distance (Å)	2.30		2.40	
$[Hg(H_2O)_2]^{2+}$	RVS	S/G-1	RVS	S/G-1
E_{MTP*}	−102.9	−101.7	−91.7	−91.8
$E_{exch/rep}$	41.7	41.6	27.3	29.4
E_1	**−61.3**	**−60.2**	**−64.4**	**−62.4**
E_{pol*}	−46.9	−42.0	−40.9	−38.1
E_{pol} ($E_{pol\ quad}$)	−50.17	−49.0 (−7.7)	−43.1	−42.8 (−5.7)
E_{CT}	−17.0	−16.7	−14.8	−14.9
E_2	**−67.2**	**−65.8**	**−57.9**	**−57.7**
ΔE	***−128.4***	***−126.0***	***−122.3***	***−120.1***

[a]Values of the QC and S/G-1 intermolecular interaction energies and their individual contributions. The Hg−O distances are in the 2.1−2.4 Å range.

Table 4. Polyligated Hg(II) Complexes[a]

$[Hg(H_2O)_4]^{2+}$ Td d(Hg−O) = 2.3 Å	RVS	S/G-1
E_{MTP*}	−194.2	−196.1
$E_{exch/rep}$	78.0	81.8
E_1	**−116.2**	**−114.3**
E_{pol*}	−72.7	−69.1
E_{pol} ($E_{pol\ quad}$)	−66.1	−62.1 (0.1)
E_{CT}	−21.4	−24.5
E_2	**−87.5**	**−86.6**
ΔE	***−203.7***	***−200.9***
$[Hg(H_2O)_6]^{2+}$ d(Hg−O) = 2.4 Å	RVS	S/G-1
E_{MTP*}	−260.0	−266.04
$E_{exch/rep}$	91.9	101.3
E_1	**−168.0**	**−164.8**
E_{pol*}	−76.0	−75.9
E_{pol} ($E_{pol\ quad}$)	−64.1	−62.0 (0.0)
E_{CT}	−19.5	−27.8
E_2	**−83.6**	**−90.1**
ΔE	***−251.6***	***−254.9***

[a](top) $[Hg(H_2O)_4]^{2+}$ in a pyramidal arrangement; (bottom) $[Hg(H_2O)_6]^{2+}$ in an octahedral arrangement. Values of the RVS and S/G-1 intermolecular interaction energies and their individual contributions.

strong improvement of charge-transfer energies. However, as explained in the technical appendix, its requires the evaluation of numerous integrals that are presently not evaluated by means of fitted densities. Work in the direction of a full density charge-transfer expression is in progress.

We studied two cases of metal cation in this article. First, Zn(II), which has predominantly a dipolar polarizability and a negligeable quadrupolar polarizability. The polarization of this cation is small in polyligated complexes because the field it undergoes from its ligands is itself very small because of their mutually canceling electric fields at its position. Its very small quadrupolar polarizability implies that it will be virtually insensitive to the magnitude of the field gradients.

Second, we addressed the case of Hg(II), which has both significant dipolar and quadrupolar polarizabilities leading to a larger cation polarization energy. In this case, the behavior of the polarization energy is more complex as it is affected by both the value of the ligands electric field and electric field gradients. Overall, a robust force field needs to address these various situations where physics at play is different for rather similar complexes.

Further developments will be dedicated to the accurate modeling of open-shell metal cations and to the generalization of the hybrid S/G-1 method enabling full GEM−GEM and S/G-1−SIBFA inter- and intramolecular computations on large and complex molecules such as proteins and nucleic acids. To conclude, thanks to the somewhat simple formalism, the inclusion of a "GEM cation" into molecular mechanics is not limited to SIBFA. Methods using the point dipole polarization approximation such as the effective fragment potential (EFP)[44] or AMOEBA[28,45] could be improved by adding such local contributions in order to deal with metals. We are currently testing such a procedure in the context of AMOEBA, through the recently introduced GEM* model.[10]

Of course, there exist alternatives to S/G-1 and AMOEBA in the context of molecular dynamic such as Drude models,[46] but as AMOEBA, they do not include charge transfer and higher order polarizabilities. Moreover, they do not aim at a term-to-term identification of the energy contributions to their QC counterpart. SCC-DFTB[47] is a promising alternative, and it would be highly instructive to evaluate its accuracy on large model complexes of Zn(II). Also, polarization effects can extend far from the recognition site. This was recently shown in the case of polarized water networks within and around recognition sites of a metalloenzymes,[48] and it could be safe to have alternative to classical QM/MM enabling to account for these at arbitrary distance.

In term of perspectives, first, both the full GEM and the hybrid S/G-1 schemes integrating a charge-transfer contribution should enable improved predictions on structural and dynamical properties of metal cations in water and metalloproteins as its gradients were recently coded (Narth et al., to be published). It should open the possibility of large-scale molecular dynamics as the possible use of Gaussian Hermite functions for simulations has been recently demonstrated (see the GEM* model,[10] implemented in Amber). Second, the models will benefit from recent advances in MPI parallelism, as new scalable strategies are now possible for the computation of the polarization energy[49] with gains going from 2 to 3 orders in magnitude in time within the Tinker framework. Overall, efforts will be devoted to propose a scalable integrated methodology incorporating both distributed multipoles and Hermite Gaussian densities in popular packages. Such a methodology could provide an alternative to emerging QM-based force fields such as mDC,[50,51] X-Pol,[52,53] or Krigin-based approach.[54]

TECHNICAL APPENDIX

A. Charge-Transfer Contribution

E_{ct} is the charge-transfer energy. Its expression has been derived from an explicit formulation proposed by Murrell et al.:[23]

$$E_{ct} = -2C \sum_{\alpha} \sum_{\beta^*} N_{occ}(\alpha) \frac{(I_{\alpha\beta^*})^2}{\Delta E_{\alpha\beta^*}} \quad (1)$$

dx.doi.org/10.1021/jp5051657 | J. Phys. Chem. A 2014, 118, 7598−7612

In the present appendix we summarize, for the first time, the present implementation of the charge-transfer contribution within the SIBFA and S/G-1 approaches. The interested reader could refer to ref 22.

In eq 1, $N_{occ}(\alpha)$ is the occupation number of the lone pair and C is a constant. α denotes the occupied orbital of the electron donor fragment A, and β^* denotes the virtual orbital of the electron acceptor fragment B. It is possible to approximate α as the lone pair carried by the atom a of the fragment A when expressed in a standard hybrid form:

$$\alpha_a = C_s 2s_a + C_p 2p_a \tag{2}$$

where the direction of each hybrid is defined by the position of its barycenter L_A. It is possible to restrict β^* to the virtual orbital of the bonds linking a hydrogen to an atom b of the fragment B. An additional approximation state

$$\beta^* = \varphi - 2s_b \tag{3}$$

with φ being the atomic orbital on h.

$\Delta E_{\alpha\beta^*}$ represents the energy difference between an electron going from the lone pair L_α of fragment A to the virtual orbital β^* of B:

$$\Delta E_{\alpha\beta^*} = (I_{L\alpha} + \sum_C V_{C\to A}) - (A_{\beta^*} + \sum_C V_{C\to B}) \tag{4}$$

$I_{L\alpha}$ being the ionisation potential of lone pair L_α, A_{β^*} the electronic affinity of the electron acceptor, and $V_{C\to A}$ and $V_{C\to B}$ are the electrostatic potential created by every fragment C on A or B.

$I_{\alpha\beta^*}$ is a function of the self-potential of orbital α and of the overlap between α and β^*, which in Dirac's notation gives

$$I_{\alpha\beta^*} = -\langle\alpha|V|\beta^*\rangle + \langle\alpha|\beta^*\rangle\langle\alpha|V|\alpha\rangle \tag{5}$$

where V is the potential generated by the electron acceptor fragment B.

In order to simplify these integrals, the $2p_a$ orbital has been developed into a component along the direction between atoms a and b (or a and h) $2p_{a\sigma}$ and another orthogonal to this direction, $2p_{a\pi}$:

$$2p_a = 2p_{a\sigma}\cos\omega_i + 2p_{a\pi}\sin\omega_i \tag{6}$$

i being either h or b and ω_i the angle between the direction aL_α of the lone pair and the direction ai of atom i (h or b). This leads us to the following simplifications:

$$\langle 2p_a|\varphi\rangle = \langle 2p_{a\sigma}|\varphi\rangle\cos\omega_h \text{ and } \langle 2p_a|2s_b\rangle = \langle 2p_{a\sigma}|2s_b\rangle\cos\omega_b \tag{7}$$

At this point, applying all previous approximations we get

$$\begin{aligned} I_{\alpha\beta^*} = {} & C_s[\tilde{V}(\langle 2s_a|\varphi\rangle - \langle 2p_a|2s_b\rangle) - \langle 2s_a|V|\varphi\rangle \\ & + \langle 2s_a|V|2s_b\rangle] + C_p[\tilde{V}(\langle 2p_{a\sigma}|\varphi\rangle\cos\omega_h \\ & - \langle 2p_{a\sigma}|2s_b\rangle\cos\omega_b) - \langle 2p_{a\sigma}|V|\varphi\rangle\cos\omega_h \\ & + \langle 2p_{a\sigma}|V|2s_b\rangle\cos\omega_b] \end{aligned} \tag{8}$$

$I_{\alpha\beta^*}$ now only depends of the different overlap integrals. the "hybrids" integrals of V over the corresponding two-center distributions, and $\tilde{V} = \langle\alpha|V|\alpha\rangle$ the self-potential of α (or integrals of V over the distribution of α) . It is possible to simplify even more these three components.

The hybrid integrals involving in a general form of two centers a and b can be developed in terms of one-center and overlap integrals:

$$\langle a|V|b\rangle = d_{ab}\langle a|V|a\rangle + d_{ba}\langle b|V|b\rangle \tag{9}$$

with

$$d_{ab} = t_{ab}\langle a|b\rangle \text{ and } d_{ba} = (1 - t_{ab})\langle a|b\rangle \tag{10}$$

where t_{ab} is a parameter characteristic of the couple of atoms involved.

The one-center integrals (self potential of α) can be approximated in different ways: either they are the lone pairs or molecular orbitals on b or h.

$\tilde{V}$ can be described by decomposing α into its different components and simplifying the interaction between fragments A and B into the single multipolar interaction and reducing the reasoning to its monopolar part for every atom c of B. Hence, the effect of B over A can be reduced to

$$V_{mono} = \sum_{c\in B}\frac{q_c}{r_c} \tag{11}$$

Since, for the range of distances of interest in intermolecular interactions, it has been shown[22] that penetration terms were negligible, we can assume that

$$\left\langle 2s_a\left|\frac{1}{r_c}\right|2s_a\right\rangle \approx \left\langle 2p_{a\sigma}\left|\frac{1}{r_c}\right|2p_{a\sigma}\right\rangle \approx \left\langle 2p_{a\pi}\left|\frac{1}{r_c}\right|2p_{a\pi}\right\rangle \tag{12}$$

and if adding the relation $C_s^2 + C_p^2 = 1$, after simplifications,[25,26] this results in

$$\begin{aligned} \tilde{V}_{mono} = \sum_c q_c\Bigg(\left\langle 2s_a\left|\frac{1}{r_c}\right|2s_a\right\rangle + 2C_sC_p\cos(\omega_c) \\ \left\langle 2s_a\left|\frac{1}{r_c}\right|2p_{a\sigma}\right\rangle\Bigg) \end{aligned} \tag{13}$$

Considering now that the second term of the expression, which is of dipolar nature, varies in $1/r^2$, while the first one, of monopolar nature, only varies in $1/r$, it appears distinctly, at the considered distances, that the last term on the right-hand side can be neglected. This gives, for the monopolar part, the relatively simple expression:

$$\tilde{V}_{mono} \approx \langle 2s_a|V|2s_a\rangle \approx \langle 2p_{a\sigma}|V|2p_{a\sigma}\rangle \tag{14}$$

Assuming a similar relationship for higher moment terms, we finally get

$$\tilde{V} \approx \langle 2s_a|V|2s_a\rangle \approx \langle 2p_{a\sigma}|V|2p_{a\sigma}\rangle \tag{15}$$

where V is describing only the multipolar interactions between fragments.

The multipolar approximation cannot be used when calculating the effects of V on its own atoms h or b because of the too short distances involved when dealing with intramolecular interactions. These integrals can be summed up into the action of h on h or of h on b. A more accurate approximation is then used to better reproduce the interactions of the nuclear charges and the electronic populations with the orbital (here on the example of h):

dx.doi.org/10.1021/jp5051657 | J. Phys. Chem. A 2014, 118, 7598−7612

$$\langle 1s_h|V^h|1s_h\rangle = Z_h \int \frac{1s_h{}^2(\vec{r}_i)}{r_h} d\vec{r}_i - Q_{el}^{\ h} \int 1s_h{}^2(\vec{r}_i) \int \frac{1s_h(\vec{r}_i)1s_h(\vec{r}_j)}{|\vec{r}_i - \vec{r}_j|} d\vec{r}_j d\vec{r}_i \quad (16)$$

If now we assume ξ_h denotes the Slater exponent on h, it is possible to expand the two different terms of the equation as a power series of ρ ($\rho = \xi_h r$) then

$$\langle 1s_h|V^h|1s_h\rangle \approx \left(\frac{3}{8}\xi_h + \frac{5}{8}\xi_h q_h\right) = F_h \quad (17)$$

for b we get

$$\langle 2s_b|V^h|2s_b\rangle = \frac{1}{n_b n_h} \sum_i F_{h,i} = F_b \quad (18)$$

where n_b is the total number of bonds on b, n_h the number of h atoms bound to b, and $F_{h,i}$ their corresponding F_h values (see ref 22 and references therein).

The overlap integrals can be simplified if considering that for the distances under consideration, the $2p_a$ overlap integrals are proportional to the corresponding $2s_a$ integrals:

$$\langle 2p_{a\sigma}|1s_h\rangle = m_{ah}\langle 2s_a|1s_h\rangle$$
$$\langle 2p_{a\sigma}|2s_b\rangle = m_{ab}\langle 2s_a|2s_b\rangle \quad (19)$$

The m values are tabulated values (see appendix in ref 22b).

The second simplification is to approximate the overlap integrals of spherical orbitals with an exponential dependence:

$$\langle\alpha|\beta\rangle \approx \exp(-\eta\rho_{ab}) \text{ with } \rho_{ab} = \frac{r_{ab}}{4\sqrt{U_a U_b}} \quad (20)$$

with α and β denoting the orbitals of atoms a and b, r_{ab}, the interatomic distance, and U_a (respectively, U_b) the effective radii of a and b corrected to fit better ab initio results:

$$U_i = U_i^0 + I((|E_\alpha| - J|E_{\beta^*}|)^2)|\cos(\omega_{\alpha\beta^*})| \quad (21)$$

Finally we get the following expression:

$$I_{\alpha\beta^*} = \exp(-\eta\rho_{ah})(D_1F_h - \tilde{V})(C_s t_{ah} + C_p m_{ah} t_{ah} \cos\omega_h) - \exp(-\eta\rho_{ab})(D_2F_b - \tilde{V})(C_s t_{ab} + C_p m_{ab} t_{ab} \cos\omega_h) \quad (22)$$

where D_1 and D_2 are adjustable parameters.

B. Polarization Energy

E_{pol} is the polarization energy. Anisotropic polarizabilities (denoted $\alpha_P(i,j)$) are used. They are distributed on the centroids of the localized orbitals and have been computed using a procedure of Garmer and Stevens.[19] Their interactions with the electrostatic fields create induced dipole moments $\Delta\mu_P(i)$ (i being x, y, or z):

$$\Delta\mu_P(i) = \sum_j^{xyz} (\alpha_P(i,j)E_P(j)) \quad (23)$$

where $E_P(j)$ is the electrostatic field generated by every point Q of every fragment B (interacting with A) inducing an electrostatic field on P:

$$E_P(j) = \sum_{B\neq A} \left(\sum_{Q\in B} E_{Q\to P}\right) \quad (24)$$

and $E_{Q\to P}$ is a damped applied electric field, which following ref 18, is modified by the following Gaussian screening function:

$$E_{Q\to P} = (1 - S(Q, P))E'_{Q\to P} \text{ with } S(Q, P) = q_Q E \exp[-F(R_{PQ}{}^2)/(V_P + V_Q)] \quad (25)$$

where q_Q is the (partial) charge of the point Q, F and E are scaling factors, R_{PQ} is the distance between the points P and Q, and V_P and V_Q are the effective radii of, respectively, points P and Q. It is important to note that $E'_{Q\to P}$ is the sum of the initial field perturbed by the external electric field

$$E'_{Q\to P}(j) = E'(\Delta\mu_Q(j)) + E'^0_{Q\to P}(j) \quad (26)$$

where $E'(\Delta\mu_Q(j))$ is the electric field created by the induced dipole and $E'^0_{Q\to P}$ is the initial field in the absence of any external field. The electric field affects the V_P and V_Q effective radii. This effect has been mimicked in ref 18 by modulating their values by an amount proportional to the dipole moment corresponding to

$$V_P = V_P^0 + G|\Delta\mu_P| \quad (27)$$

where E, F, and G are adjustable parameters and V_P^0 is the effective radius in absence of any external field.

The polarization energy is then

$$E_{pol}(P) = -0.5 \sum_i^{xyz} \Delta\mu_P(i)(E_P(i))^0 \quad (28)$$

where E^0 denotes the electrostatic field due to the permanent multipoles.

Such an iterative process for the electric field and effective radii acts as a more realistic "expansion/compression" model where the interactions between polarized centers in return influence the values of the effective radii, which act on the polarization energy itself. Overall, thanks to the damping associated with the compression-like model, the SIBFA polarization embodies altogether the exchange-polarization effects as well as all present quantum effects. Therefore, the parameterization of the model needs to be grounded on a reference ab initio decomposition method such as RVS, which includes exchange-polarization effects within the polarization through a consistent use of antisymmetrized wavefunctions.

C. Ab Initio Parametrization of E_{pol} and E_{ct}

E_{pol^*}/E_{pol} and E_{ct} are presently taking care of the nonadditive effects within SIBFA and S/G-1. The values for E_{pol^*} and E_{ct} are presently consistent with the RVS ones and correspond to the energy obtained after the first iteration of the induced dipoles. Nevertheless, $E_{pol^*}{}^{RVS}$ does not include higher order polarization terms, such as the quadrupolar polarization terms ($E_{pol\ quad}$), leading to the final relaxed E_{pol}. In SIBFA, the E_{pol} values are computed through converging the iterative induced dipoles cycles. The ab initio values can be approximated by computing E_{pol^*} as

$$E_{pol}(QC) = \Delta E_{tot}(RVS) - E_1(RVS) - E_{ct}(RVS) \quad (29)$$

The BSSE correction that is included in the final interaction energy (ΔE_{tot}) is taken into account within the charge-transfer energy:

$$E_{CT}(SIBFA) = E_{CT}(RVS) + BSSE \quad (30)$$

These final equations lead to

dx.doi.org/10.1021/jp5051657 | J. Phys. Chem. A 2014, 118, 7598−7612

$$\begin{aligned}\Delta E_{tot}(\text{SIBFA}) &= E_1(\text{SIBFA}) + E_2(\text{SIBFA})\\ &= E_{Coul}(\text{SIBFA}) + E_{exch\text{-}rep}(\text{SIBFA})\\ &\quad + E_{pol}(\text{SIBFA}) + E_{CT}(\text{SIBFA})\\ \Delta E(\text{QC}) &= E_{Coul}(\text{RVS}) + E_{exch\text{-}rep}(\text{RVS})\\ &\quad + [\Delta E_{tot}(\text{RVS}) - E_1(\text{RVS})\\ &\quad - E_{CT}(\text{RVS})] + [E_{CT}(\text{RVS}) + \text{BSSE}]\\ &= \Delta E_{tot}(\text{RVS}) + \text{BSSE}\\ &= \Delta E_{tot}(\text{RVS}-\text{BSSE corrected})\end{aligned} \tag{31}$$

■ ASSOCIATED CONTENT

Supporting Information

Data tables. This material is available free of charge via the Internet at http://pubs.acs.org.

■ AUTHOR INFORMATION

Corresponding Authors

*(G.A.C.) E-mail: andres@chem.wayne.edu.
*(J.-P.P.) E-mail: jpp@lct.jussieu.fr.

Notes

The authors declare no competing financial interest.

■ ACKNOWLEDGMENTS

Support from the French National Research Agency (ANR) is acknowledged (Grant ANR-08-BLAN-0158), as well as computer time allowances by CRIHAN (Rouen, France, Project 2008011) and GENCI (IDRIS, CINES, France, project x2010075027). This work was also supported by the French state funds managed by CALSIMLAB and the ANR within the Investissements d'Avenir program under reference ANR-11-IDEX-0004-02. Support from Wayne State University is gratefully acknowledged. One of us (J.-P.P.) thank Ken Jordan for enlightening discussions and for a long-standing collaboration in the organization of TSRC workshops.

■ REFERENCES

(1) Brooks, B. R.; Brooks, C. L.; Mackerell, A. D.; Nilsson, L.; Petrella, R. J.; Roux, B.; Won, Y.; Archontis, G.; Bartels, C.; Boresch, S.; Caflisch, M.; et al. CHARMM: the Biomolecular Simulation Program. *J. Comput. Chem.* **2009**, *30*, 1545−1614.

(2) Case, D. A.; Cheatham, T. E.; Darden, T.; Gohlke, H.; Luo, R.; Merz, K. M.; Onufriev, A.; Simmerling, C.; Wang, B.; Woods, R. J. The Amber Biomolecular Simulation Programs. *J. Comput. Chem.* **2005**, *26*, 1668−1688.

(3) Oostenbrink, C.; Villa, A.; Mark, A. E.; Van Gunsteren, W. F. A Biomolecular Force Field based on the Free Enthalpy of Hydration and Solvation: The GROMOS Force-Field Parameter Sets 53A5 and 53A6. *J. . Comput. Chem.* **2004**, *25*, 1656−1676.

(4) Gresh, N.; Cisneros, G. A.; Darden, T. A.; Piquemal, J.-P. Anisotropic, Polarizable Molecular Mechanics Studies of Inter- and Intramolecular Interactions and Ligand−Macromolecule Complexes. A Bottom-Up Approach. *J. Chem. Theory Comput.* **2007**, *3*, 1960−1986.

(5) de Courcy, B.; Piquemal, J.-P.; Gresh, N. Energy Analysis of Zn Polycoordination in a Metalloprotein Environment and of the Role of a Neighboring Aromatic Residue. What Is the Impact of Polarization? *J. Chem. Theory Comput.* **2008**, *4*, 1659−1668.

(6) Jenkins, L.; Hara, T.; Durell, S.; Hayashi, R.; Inman, J.; Piquemal, J.; Gresh, N.; Appella, E. Specificity of Acyl Transfer from 2-Mercaptobenzamide Thioesters to the HIV-1 Nucleocapsid Protein. *J. Am. Chem. Soc.* **2007**, *129*, 11067−11078.

(7) Marjolin, A.; Gourlaouen, C.; Clavaguera, C.; Gresh, N.; Ren, P. Y.; Wu, J.; Dognon, J.-P.; Piquemal, J.-P. Toward Accurate Solvation Dynamics of Lanthanides and Actinides in Water using Polarizable Force Fields: from Gas-Phase Energetics to Hydration Free Energies. *Theor. Chem. Acc.* **2012**, *131*, 1198.

(8) Piquemal, J. P.; Cisneros, G. A.; Reinhardt, P.; Gresh, N.; Darden, T. A. Towards a Force Field based on Density Fitting. *J. Chem. Phys.* **2006**, *124*, 104101.

(9) Cisneros, G. A.; Piquemal, J.-P.; Darden, T. Generalization of the Gaussian Electrostatic Model: Extension to Arbitrary Angular Momentum, Distributed Multipoles and Speedup with Reciprocal Space Methods. *J. Chem. Phys.* **2006**, *125*, 184101.

(10) Duke, R.; Starovoytov, O.; Piquemal, J.-P.; Cisneros, G. A. GEM*: A Molecular Electronic Density-Based Force Field for Classical Molecular Dynamics Simulations. *J. Chem. Theory Comput.* **2014**, *10*, 1361−1365.

(11) Cisneros, G. A.; Piquemal, J.-P.; Darden, T. A. QM/MM Electrostatic Embedding with Continuous and Discrete Functions. *J. Phys. Chem. B* **2006**, *110*, 13682−13684.

(12) Vigné-Maeder, F.; Claverie, P. The Exact Multicenter Multipolar Part of a Molecular Charge Distribution. *J. Chem. Phys.* **1988**, *88*, 4934.

(13) Piquemal, J.-P.; Gresh, N.; Giessner-Prettre, C. Improved Formulas for the Calculation of the Electrostatic Contribution to Intermolecular Interaction Energy from Multipolar Expansion of the Electronic Distribution. *J. Phys. Chem. A* **2003**, *107*, 10353−10359.

(14) Murrell, J. N.; Teixeira, J. Dependence of Exchange Energy on Orbital Overlap. *J. Mol. Phys.* **1970**, *19*, 521.

(15) Williams, D. R.; Schaad, L. J.; Murrell, J. N. Deviations from Pairwise Additivity in Intermolecular Potentials. *J. Chem. Phys.* **1967**, *47*, 4916.

(16) Piquemal, J.-P.; Chevreau, H.; Gresh, N. Towards a Separate Reproduction of the Contributions to the Hartree-Fock and DFT Intermolecular Interaction Energies by Polarizable Molecular Mechanics with the SIBFA Potential. *J. Chem. Theory. Comput.* **2007**, *3*, 824−837.

(17) Chaudret, R.; Gresh, N.; Parisel, O.; Piquemal, J.-P. Many-body Exchange-Repulsion in Polarizable Molecular Mechanics. I. Orbital based Approximations and Application to Hydrated Metal Cations Complexes. *J. Comput. Chem.* **2011**, *32*, 2949−2957.

(18) Gresh, N. Energetics of Zn Binding to a Series of Biologically Relevant Ligands. *J. Comput. Chem.* **1995**, *16*, 856−882.

(19) Garmer, D. R.; Stevens, W. J. Transferability of Molecular Distributed Polarizabilities from a Simple Localized Orbital based Method. *J. Phys. Chem.* **1989**, *93*, 8263−8270.

(20) Dupuis, M.; Marquez, A.; Davidson, E. R. *HONDO 95.3 QCPE*; Indiana University: Bloomington, IN, 1995.

(21) Piquemal, J.-P.; Chelli, R.; Procacci, P.; Gresh, N. Key Role of the Polarization Anisotropy of Water in Modeling Classical Polarizable Force Fields. *J. Phys. Chem. A* **2007**, *111*, 8170−8176.

(22) (a) Gresh, N.; Claverie, P.; Pullman, A. Computations of intermolecular interactions. Expansion of a charge-transfer energy contribution in the framework of an additive procedure. Applications to hydrogen-bonded systems. *Int. J. Quantum Chem.* **1982**, *22*, 199−215. (b) Gresh, N.; Claverie, P.; Pullman, A. Intermolecular Interactions: Elaboration on an Additive Procedure including an Explicit Charge-Transfer Contribution. *Int. J. Quantum Chem.* **1986**, *29*, 101−118.

(23) Murrell, J. N.; Randic, M.; Williams, D. R. The Theory of Intermolecular Forces in the Region of Small Orbital Overlap. *Proc. R. Soc. London A* **1965**, *284*, 566−581.

(24) Wheatley, R. J.; Price, S. An Overlap Model for Estimating the Anisotropy of rRpulsion. *Mol. Phys.* **1990**, *69*, 507−533.

(25) Dunlap, B. I.; Connolly, J. W. D.; Sabin, J. R. On First Row Diatomic Molecules and Local Density Models. *J. Chem. Phys.* **1979**, *71*, 4993.

(26) Boys, S. F.; Shavitt, I. *Report WIS-AF-13, NTIS AD212985*, 1959.

(27) McMurchie, L. E.; Davidson, E. R. One- and Two-electron Integrals over Cartesian Gaussian Functions. *J. Comput. Phys.* **1978**, *26*, 218−231.
(28) Ponder, J. W.; Wu, C.; Ren, P.; Pande, V. S.; Chodera, J. D.; Schnieders, M. J.; Haque, I.; Mobley, D. L.; Lambrecht, D. S.; DiStasio, R. A., Jr.; Head-Gordon, M.; Clark, G. N.; Johnson, M. E.; Head-Gordon, T. Current Status of the AMOEBA Polarizable Force Field. *J. Phys. Chem. B* **2010**, *114*, 2549−2564.
(29) Bagus, P. S.; Illas, F. Decomposition of the Chemisorption Bondconstrained Variations Order of the Variations and Construction of the Variational Spaces. *J. Chem. Phys.* **1992**, *96*, 8962.
(30) Stevens, W. J.; Fink, W. H. Frozen Fragment Reduced Variational Space Analysis of Hydrogen Bonding Interactions. Application to the Water Dimer. *Chem. Phys. Lett.* **1987**, *139*, 15−22.
(31) Gordon, M. S.; Schmidt, M. W. Advances in Electronic Structure Theory: GAMESS a Decade Later. In *Theory and Applications of Computational Chemistry, the First 40 Years*; Dykstra, C. E., Frenking, G., Lim, K. S., Scuseria, G. E., Eds.; Elsevier: Amsterdam, 2005.
(32) Schmidt, M. W.; Baldridge, K. K.; Boatz, J. A.; Elbert, S. T.; Gordon, M. S.; Jensen, J. H.; Koseki, S.; Matsunaga, N.; Nguyen, K. A.; Su, S. J.; Windus, T. L.; Dupuis, M.; Montgomery, J. A. General Atomic and Molecular Electronic Structure System. *J. Comput. Chem.* **1993**, *14*, 1347−1363.
(33) Stevens, W. J.; Basch, H.; Krauss, M. Compact Effective Potentials and Efficient Shared-Exponent Basis-Sets for the 1st-Row and 2nd-Row Atoms. *J. Chem. Phys.* **1984**, *81*, 6026.
(34) Gresh, N.; Audiffren, N.; Piquemal, J.-P.; de Ruyck, J.; Ledecq, M.; Wouters, J. Analysis of the Interactions Taking Place in the Recognition Site of a Bimetallic Mg(II)-Zn(II) Enzyme, Isopentenyl Diphosphate Isomerase. A Parallel Quantum-Chemical and Polarizable Molecular Mechanics Study. *J. Phys. Chem. B* **2010**, *114*, 4884−4895.
(35) (a) Becke, A. D. Density-Functional Exchange-Energy Approximation with Correct Asymptotic Behavior. *Phys. Rev. A* **1988**, *38*, 3098. (b) Lee, C.; Yang, W.; Parr, R. G. Development of the Colle−Salvetti Correlation-Energy Formula into a Functional of the Electron Density. *Phys. Rev. B* **1988**, *37*, 785.
(36) (a) Dunning, T. H., Jr. Gaussian Basis Sets for Use in Correlated Molecular Calculations. I. The Atoms Boron Through Neon and Hydrogen. *J. Chem. Phys.* **1989**, *90*, 1007−1023. (b) Petersson, G. A.; Bennett, A.; Tensfeldt, T. G.; Al-Laham, M. A.; Shirley, W. A.; Mantzaris, J. A Complete Basis Set Model Chemistry. I. The Total Energies of Closed-shell Atoms and Hydrides of the First-Row Atoms. *J. Chem. Phys.* **1988**, *89*, 2193−218.
(37) Cisneros, G. A.; Darden, T. A.; Gresh, N.; Pilmé, J.; Reinhardt, P.; Parisel, O.; Piquemal, J.-P. Design Of Next Generation Force Fields From Ab Initio Computations: Beyond Point Charges Electrostatics. In *Multi-Scale Quantum Models for Biocatalysis*; Springer: New York, 2009; p 137.
(38) Crabtree, R. H. *The Organometallic Chemistry of the Transition Metals*; Wiley: New York, 2009.
(39) Wu, J.; Piquemal, J.-P.; Chaudret, R.; Reinhardt, P.; Ren, P. Y. Polarizable Molecular Dynamics Simulation of Zn(II) in Water using the Polarizable AMOEBA Force Field. *J. Chem. Theory. Comput.* **2010**, *6*, 2059−2070.
(40) Frisch, M. J.; Trucks, G. W.; Schlegel, H. B.; Scuseria, G. E.; Robb, M. A.; Cheeseman, J. R.; Scalmani, G.; Barone, V.; Mennucci, B.; Petersson, G. A.; et al. *Gaussian 09*, revision D.01; Gaussian, Inc.: Wallingford, CT, 2009.
(41) Gresh, N.; Piquemal, J.-P.; Krauss, M. Representation of Zn(II) Complexes in Polarizable Molecular Mechanics. Further Refinements of the Electrostatic and Short-range Contribution of the Intermolecular Interaction Energy. Comparisons with Parallel ab Initio Computations. *J. Comput. Chem.* **2005**, *26*, 1113−1130.
(42) Buckingham, A. D. Intermolecular Forces. *Philos. Trans. R. Soc. London B* **1975**, *272*, 5−12.
(43) Gresh, N.; Policar, C.; Giessner-Prettre, C. Modeling Copper(I) Complexes: SIBFA Molecular Mechanics versus ab Initio Energetics and Geometrical Arrangements. *J. Phys. Chem. A* **2002**, *106*, 5660−5670.
(44) (a) Gordon, M. S.; Slipchenko, L. V.; Li, H.; Jensen, J. H. The Effective Fragment Potential: A General Method for Predicting Intermolecular Forces. *Annu. Rep. Comput. Chem.* **2007**, *3*, 177−193. (b) Gordon, M. S.; Smith, Q. A.; Xu, P.; Slipchenko, L. V. Accurate First Principles Model Potentials for Intermolecular Interactions. *Annu. Rev. Phys. Chem.* **2013**, *64*, 553−78.
(45) Ren, P. Y.; Ponder, J. W. Polarizable Atomic Multipole Water Model for Molecular Mechanics Simulation. *J. Phys. Chem. B* **2003**, *107*, 5933−5947.
(46) Yu, H.; Whitfield, T. R.; Harder, E.; Lamoureux, G.; Vorobyov, I.; Anisimov, V. M.; MacKerell, A. D., Jr.; Roux, B. Simulating Monovalent and Divalent Ions in Aqueous Solution using a Drude Polarizable Force Field. *J. Chem. Theory Comput.* **2010**, *6*, 774−786.
(47) Elstner, M.; Cui, Q.; Munih, P.; Kaxiras, E.; Frauenheim, T.; Karplus, M. Modeling Zinc in Biomolecules with the Self Consistent Charge-Density Functional Tight Binding (SCC-DFTB) Method: Applications to Structural and Energetic Analysis. *J. Comput. Chem.* **2003**, *24*, 565−581.
(48) Gresh, N.; de Courcy, B.; Piquemal, J.-P.; Foret, F.; Courtiol-Legourd, S.; Salmon, L. Polarizable Water Molecules in Ligand-Metalloprotein Recognition. Impact on the Relative Complexation Energies of Zn-dependent Phosphomannose Isomerase with D-Mannose 6-Phosphate Surrogates. *J. Phys. Chem. B* **2011**, *115*, 8304−8316.
(49) Lipparini, F.; Lagardere, L.; Stamm, B.; Cances, B.; Schnieders, M.; Ren, P. Y.; Maday, Y.; Piquemal, J.-P. Scalable Evaluation of the Polarization Energy and Associated Forces in Polarizable Molecular Dynamics: I. towards Massively Parallel Direct Space Computations. *J. Chem. Theory Comput.* **2014**, *10*, 1638−1651.
(50) Giese, T. J.; Chen, H. C.; Dissanayake, T.; Giambasu, G. M.; Heldenbrand, H.; Huang, M.; Kuechler, E. R.; Lee, T. S.; Panteva, M. T.; Radak, B. K.; York, D. M. A Variational Linear-Scaling Framework to Build Practical, Efficient Next-Generation Orbital-Based Quantum Force Fields. *J. Chem. Theory Comput.* **2013**, *9*, 1417−1427.
(51) Giese, T. J.; Chen, H.; Huang, M.; York, D. M. Parametrization of an Orbital-Based Linear-Scaling Quantum Force Field for Noncovalent Interactions. *J. Chem. Theory Comput.* **2014**, *10*, 1086−1098.
(52) Gao, J. Toward a Molecular Orbital Derived Empirical Potential for Liquid Simulations. *J. Phys. Chem. B* **1997**, *101*, 657−653.
(53) Han, J.; Truhlar, D. G.; Gao, J. Optimization of the Explicit Polarization (X-Pol) Potential Using a Hybrid Density Functional. *J. Theor. Chem. Acc.* **2012**, *131*, 1161.
(54) Kandathil, S.; Fletcher, T.; Yuan, Y.; Knowles, J.; Popelier, P. Accuracy and Tractability of a Kriging Model of Intramolecular Polarizable Multipolar Electrostatics and its Application to Histidine. *J. Comput. Chem.* **2013**, *34*, 1850−61.